Local Acoustic Forcing of a Wing at Low Reynolds Numbers

S. L. Yang* and G. R. Spedding†
University of Southern California, Los Angeles, California 90089-1191

DOI: 10.2514/1.J052984

At transitional Reynolds numbers ($10^4 - 10^5$), many smooth airfoils experience laminar flow separation and possible turbulent reattachment, where the occurrence of either state is strongly influenced by small changes in the surrounding environment. The Eppler 387 airfoil is one of many airfoils that can have multiple lift and drag states at a single wing incidence angle. Prestall hysteresis and abrupt switching between stable states occur due to sudden flow reattachment and the appearance of a separation bubble close to the leading edge. Here, we demonstrate control of the flow dynamics by localized acoustic excitation through small speakers embedded beneath the suction surface. The flow can be controlled not only through variations in acoustic power and frequency, but also through spatial variations in forcing location. Implications for control and stabilization of small aircraft are considered.

Nomenclature

AR	=	aspect ratio
b	=	half-span of the wing, m
C_D	=	total drag coefficient on a finite wing
C_L	=	total lift coefficient on a finite wing
c	=	chord, m
c'	=	normalized chordwise coordinate
c_s	=	separation line location, m
f_e	=	excitation frequency, Hz
f_s	=	separated shear-layer instability shedding frequency, Hz
L/D	=	lift-to-drag ratio
Re	=	chord-based Reynolds number
St	=	Strouhal number
U_0	=	freestream velocity, m/s
x, y, z	=	coordinates in streamwise, spanwise, and normal directions
α	=	angle of attack, deg
ω	=	spanwise component of vorticity, rad/s
*	=	preferential value

I. Introduction

A GROWING number of micro aerial vehicles operate in a particular flight regime where the chord-based Reynolds number $Re = U_0 c/\nu$ (where U_0 is the flight speed, c is the chord, and ν is the kinematic viscosity) lies between 10^4 and 10^5. In this regime, when flow over a surface has insufficient energy to overcome the adverse pressure gradient in the laminar boundary layer, the flow separates from the surface, undergoes transition to turbulence, and can reattach to form a laminar separation bubble. The turbulent transition leading to the formation of a laminar separation bubble has been experimentally and numerically shown [1,2] to be caused by the transformation of initially two-dimensional instabilities into three-dimensional shear-layer instabilities. The laminar separation bubble is associated with increased circulation, increasing the overall lift on an airfoil, and so separation and possible turbulent reattachment can either favorably or adversely affect wing performance. The Eppler 387 airfoil, along with many other smooth airfoils, can be in either one of two states: a low-lift state (SI in Fig. 1), where separation occurs before the trailing edge without reattachment, or a high-lift state (SII), where initial separation is followed by the formation of a laminar separation bubble and flow reattachment. A number of intrinsic unstable modes in the laminar separation bubble problem have been identified [3–5], from Tollmien–Schlichting waves in the still-attached, laminar boundary layer to Kelvin–Helmholtz instabilities in the later separated shear layer, together with possible mixed modes in between. Several of these modes are known to be susceptible to acoustic perturbation, and we propose to exploit this to test the possibility of active control between the SI and SII flow states.

Previous tests of acoustic excitation in the Dryden Wind Tunnel involved acoustically exciting a E387 wing by a speaker that was placed on the outside of the wind-tunnel test section, turning the entire test section into a resonating chamber [6]. Acoustic forcing of the flow around an E387 wing at $Re = 40,000$ and 60,000 at certain excitation frequencies f_e increased lift at certain angles of attack, tripped the flow from low- to high-lift state (SI-SII), eliminated prestall hysteresis, and promoted flow reattachment. In an enclosed chamber, minima in the rms acoustic power correspond to minimum fluctuating pressure and maximum velocity fluctuations, and external acoustic excitation at values of f_e that correlated with test section antiresonances yielded the largest improvement in L/D. It was also shown that a harmonic of one of these optimum excitation frequencies matched the shear-layer instability frequency f_s, suggesting that the flow over the wing is altered when acoustic excitation matches a naturally occurring instability in the shear layer.

Internal acoustic excitation of airfoils and wings has been shown to increase lift and delay and/or prevent separation, sensitive to both excitation frequency and sound pressure level (SPL) [7–11]. The most common internal acoustic forcing experiment has a speaker inside the wing with spanwise slots so that sound travels through the entire span of the wing, exiting at the open slot(s), and it has been shown [8,11] that acoustic forcing is most effective when applied at a point $x'/c = c'$ close to or before the chordwise separation point c_s, so that $x' \leq c_s$.

The effect of acoustic forcing was found to deteriorate as c' moved farther from c_s, and forcing aft of c_s required considerably higher SPL to achieve the same reduction in L/D. However, the optimum values of forcing frequency f_e^* were reported to be independent of c' [8]. When excitation was forced near c_s, f_e^* was found to be equal to the separated shear instability frequency f_s or a subharmonic [8,10].

Tests from both external and internal acoustic forcing show that the values of f_e^* correspond to the dominant natural instabilities in the separated region. A nondimensional Strouhal number St can be written as

$$St = \frac{f_e c}{U_0} \tag{1}$$

Presented as Paper 2013-2747 at the 43rd AIAA Fluid Dynamics Conference, San Diego, CA, 24–27 June 2013; received 13 August 2013; revision received 19 November 2013; accepted for publication 9 January 2014; published online 23 April 2014.

*Department of Aerospace and Mechanical Engineering; shanling.yang@usc.edu. Member AIAA.

†Professor, Department of Aerospace and Mechanical Engineering; geoff@usc.edu. Member AIAA.

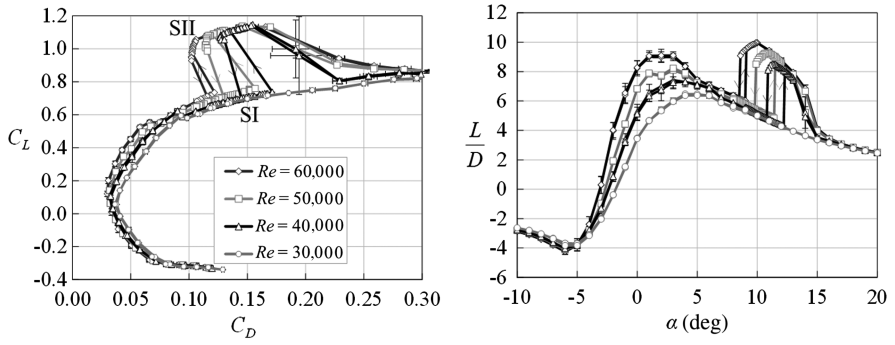

a) b)

Fig. 1 $C_L(C_D)$ and L/D curves show bi-stable states for the E387 wing at various Re.

If the main frequency selection depends on length scales in the viscous boundary layer or in the separated shear layer, then a modified Strouhal number $St^* = St/Re^{1/2}$ may be relevant. However, studies of internal acoustic forcing at both transitional and moderate Re show a large range of St^* from 0.001 to 0.04, with subranges specific to particular wing α [8–10], and generally applicable scaling laws may be elusive.

This paper provides a study on the effects of internal acoustic excitation on the forces and flowfields of an E387 wing in an Re regime where prestall hysteresis and abrupt switching of bistable states occur. This study is the continuation of a series of experiments to acoustically excite the boundary-layer instabilities and control flow separation of wings at transitional Re. As an extension of the external acoustic forcing tests, the experiments reported here aim to eliminate the role of global standing waves that inevitably occur with facility-dependent resonances by truly localizing the acoustic forcing. Applications of this research to small-scale aircraft could lead to energy-efficient separation control as well as overall aerodynamic improvement with no moving parts.

II. Materials and Methods

A. Wind Tunnel and Instrumentation

Experiments were performed in the Dryden wind tunnel at the University of Southern California. Lift and drag forces were measured with a custom force balance (described in detail in previous experiments [12–14]) placed below the wind-tunnel floor. Particle image velocimetry (PIV) was used to estimate velocity components (u, w) in the two-dimensional plane (x, z) with the same setup used by Yang and Spedding [15] (Fig. 2) but with an improved resolution Imager Pro X 2M (1648 × 1214 × 14 bit) camera.

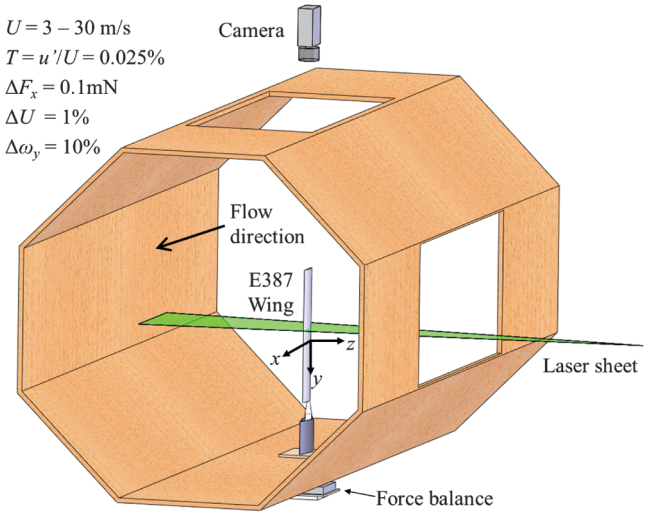

Fig. 2 Wind tunnel setup. (x, y, z) are streamwise, spanwise, and normal directions. Origin is at leading edge and midspan.

B. Acoustic Equipment

The internal sound sources were Knowles Acoustics wideband FK series speakers with dimensions 6.50 × 2.75 × 1.95 mm, with a frequency response of 4001000 Hz ±3 dB. EX1200-3608 16 bit digital-to-analog converters were used to generate sine waves with adjustable frequency and amplitude, and these were amplified with Kramer VA-16XL variable-gain stereo audio amplifiers with a ±3 dB frequency range of 20 Hz40 kHz.

C. Wing Model

The wing model had an Eppler 387 profile (inset of Fig. 3a) with an aspect ratio AR = 6 (span $2b = 54$ cm and chord $c = 9$ cm). The model was a two-part aluminum wing composed of a base and a lid, as shown in Fig. 3. The base of the wing contained cavities and channels into which speakers and wires were embedded. The lid, which contained 0.5-mm-diam holes for sound emission, slid over and locked into the base by a tongue-and-groove connection. The model had a total of 180 speaker cavities arranged in six rows, each with 30 cavities, as noted in Fig. 3b. The individual holes in the wing suction surface were either covered with tissue paper diaphragms from the underside of the lid, leaving cavities of width-to-depth ratio of 1/2, or filled in with modeling clay.

III. Results

A. Baseline Performance of the Eppler 387 Wing

Cavities with a width-to-height ratio of 1/2 do not affect the basic performance of the wing [15], and the perforated wing with holes covered from the bottom of the lid performed the same as a solid wing of the same size, used in prior external acoustic forcing experiments [6]. The standard behavior of the wing at these transitional Re includes the sudden jump from the low-lift (SI) state to high-lift (SII)

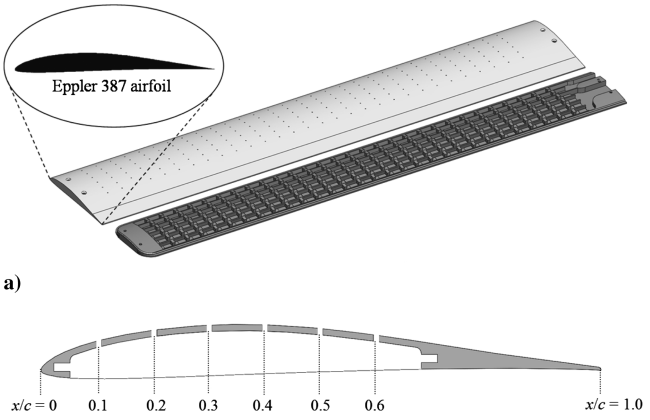

a) b)

Fig. 3 a) Two-piece E387 wing, and b) profile view of the lid. Spanwise rows of holes are located at $x/c = \{0.1, 0.2, 0.3, 0.4, 0.5, 0.6\}$. From Yang et al. [15].

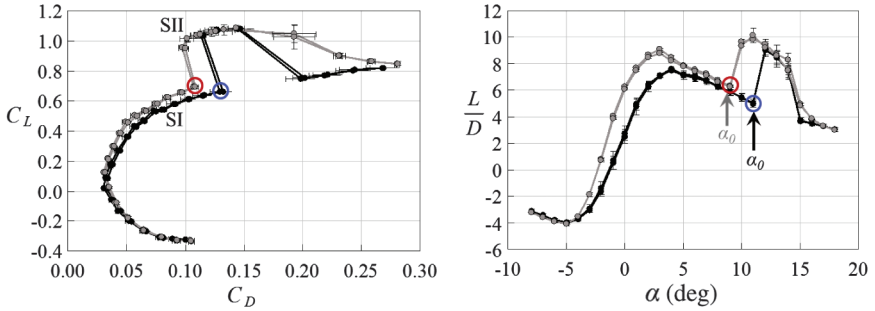

Fig. 4 $C_L(C_D)$ curves and L/D curves for the E387 at $Re = 40{,}000$ (black) and 60,000 (gray) without excitation.

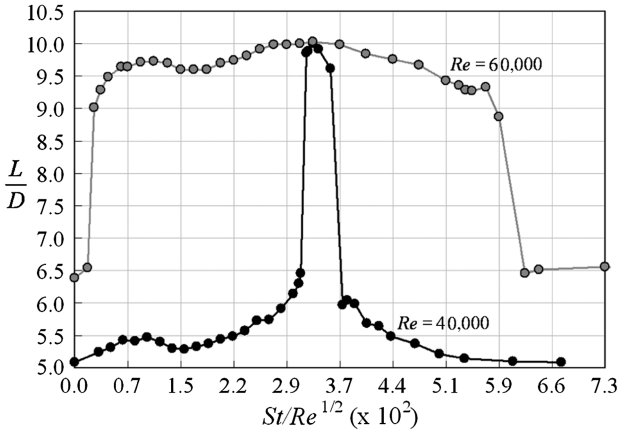

Fig. 5 L/D at $Re = 40{,}000$, $\alpha = 11$ deg (black), $Re = 60{,}000$, $\alpha = 9$ deg (gray), resulting from excitation at different St^*. Excitation occurs at constant amplitude settings.

state at a prestall angle of attack, as seen in Fig. 4. At $Re = 40,000$, with external acoustic forcing, the current wing had values of f_e^* similar to the solid E387 wing, with the two most effective frequencies being 420 and 520 Hz ($St^* = 0.028$ and 0.035, respectively).

B. Excitation at Different Reynolds Numbers

In initial tests, 15 speakers were activated (phase-synchronized in time) over $-0.83 \le y/b \le 0.83$ and spaced $\Delta(y/b) = 0.12$ apart at the chordwise excitation location $c' = 0.1$. Lift and drag forces were measured for a series of different excitation frequencies f_e at a pre-SII angle of attack α_0 for $Re = 40,000$ and 60,000 (as noted in Fig. 4). The changes in L/D from internal forcing at $c' = 0.1$, shown in Fig. 5, show that, at $Re = 40,000$, a single optimum excitation value occurs at 500 Hz ($St^* = 0.034$), for $\Delta(L/D) \approx 97\%$. On the other hand, at $Re = 60,000$, a broad range of f_e exists between 200 $\le f_e \le$ 1500 Hz ($0.007 \le St^* \le 0.055$), for $\Delta(L/D) \approx 57\%$. L/D at $f_e = 500$ Hz is about the same, regardless of Re. $L/D(\alpha)$ at $Re = 40,000$ and 60,000 are shown in Fig. 6. Improvements in L and D occur within a small range of low, prestall α where the bistable states exist (5–11 deg for $Re = 40,000$, and 2–10 deg for $Re = 60,000$).

C. Spanwise Distribution

Until now, internal acoustic forcing was always applied uniformly across the span [7–11], though it is well known that three-dimensional instabilities can rapidly promote transition to turbulence in otherwise nominally two-dimensional structures, such as mixing layers [16–19]. The possible role of spanwise forcing variation in influencing three-dimensional transition was examined at $Re = 60,000$ and $\alpha_0 = 9$ deg. Speakers located at $c' = 0.1$ and spaced evenly were forced at $f_e = 800$ Hz ($St^* = 0.029$). The different span fractions of activated speakers were 0, 12, 24, 36, 48, and 83% of the total span, centered about midspan. Figure 7 shows that, between the extreme configurations (one speaker at $y/b = 0$ and 15 speakers between $-0.83 \le y/b \le 0.83$), a family of curves exists and that a broader spanwise coverage produces improved aerodynamic performance. Note that two effects are combined here: an increase in spanwise coverage and simply a larger number of speakers, and hence a higher acoustic power input to the flow. Figure 8 expresses the nearly linear relation between increase in $\Delta(L/D)$ and number of speakers.

One can also vary the number of speakers in a fixed span fraction, and Fig. 9 shows the variation in L/D as a function of number of speakers, or speaker density, over $-0.36 \le y/b \le 0.36$. Increasing the number of speakers (with decreased spacing between them) results in a higher $\Delta(L/D)$. Figure 10 once again shows a correlation of increasing wing performance with increasing number of speakers, but this correlation is not as linear as for the varying spanwise distribution with constant spacing (Fig. 8), and so although $\Delta(L/D)$ varies with the spanwise distribution of sound sources, it depends also on their density. Although the configuration yielding the greatest performance improvement would be a continuous line source (where the limit of $\Delta(y/b)$ goes to zero), the optimum efficiency in terms of

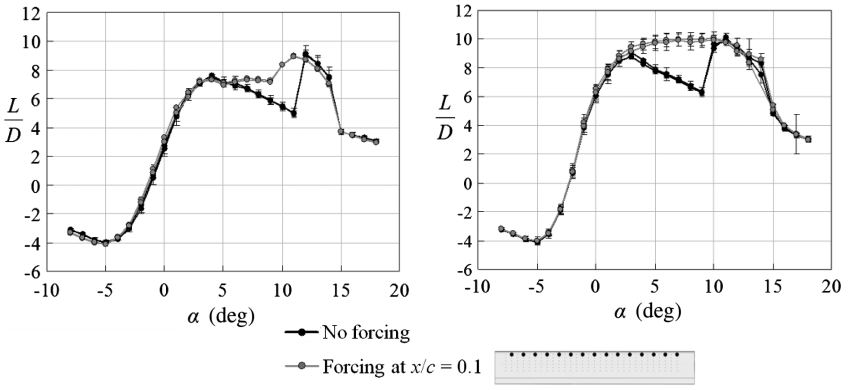

a) b)

Fig. 6 L/D for the E387 wing at a) $Re = 40,000$ with and without excitation at $f_e = 500$ Hz ($St^* = 0.034$), and b) $Re = 60,000$ with and without excitation at $f_e = 800$ Hz ($St^* = 0.029$).

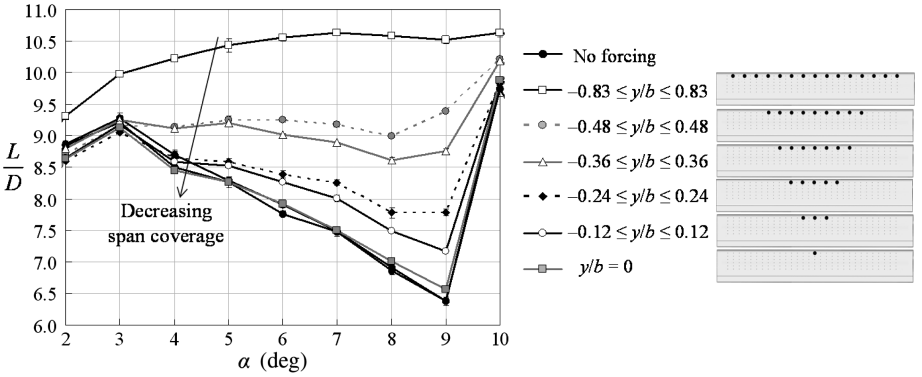

Fig. 7 L/D for the E387 wing at $Re = 60{,}000$ for different spanwise distributions of activated speakers. Forcing is at $f_e = 800$ Hz ($St^* = 0.029$).

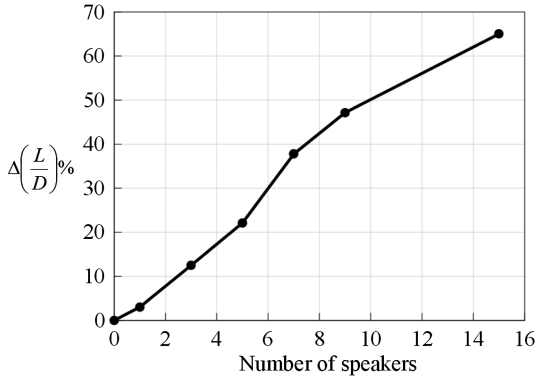

Fig. 8 $\Delta(L/D)$ for the E387 wing at $Re = 60{,}000$ and $\alpha = 9$ deg for varying number of speakers spaced evenly apart, forced at $f_e = 800$ Hz ($St^* = 0.029$).

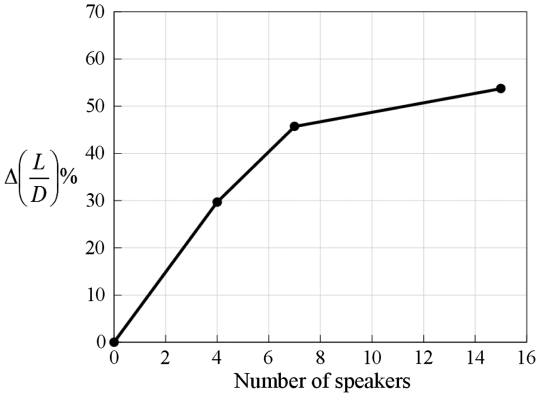

Fig. 10 $\Delta(L/D)$ for the E387 wing at $Re = 60{,}000$ and $\alpha = 9$ deg for varying number of speakers and fixed span coverage, forced at $f_e = 850$ Hz ($St^* = 0.031$).

excitation energy versus propulsion energy requirement would be some intermediate value that exploits the finite area of a nominally local excitation source. It is not yet clear whether the optimum spanwise spacing that would be found corresponds to a natural three-dimensional mode in the separated, or bubble, shear layer or whether it simply reflects the finite area influenced by the acoustic waves as they propagate from the small source through the shear layer. Experiments to verify this might involve deliberate three-dimensional geometric forcing of the flow at one wavelength and varying the spanwise wavelength of acoustic excitation sources around that.

D. Amplitude Variation

External acoustic excitation of the same E387 wing [6] and reports on internal acoustic excitation of others [7,6,9–11] showed that $\Delta(L/D)$ varies predictably with acoustic forcing amplitude. Similar to Fig. 7, the number of activated speakers at $c' = 0.1$ was varied, but the number of diaphragms was kept constant. Though the chambers beneath each speaker in the wing could be mechanically sealed, we cannot be sure that they were acoustically isolated, and so inactive diaphragms could still act as passive acoustic sources. Figure 11 can be compared with Fig. 7, where the inactive speaker locations had no diaphragm. The entire baseline $\Delta(L/D)$ is raised, and small, and local forcing can have a pronounced effect on global L/D. For example, the effectiveness of single speaker forcing when surrounded by passive diaphragms is much greater; at $\alpha = 8$ deg, $L/D \approx 9$, a result that is only achieved with a row of nine speakers in Fig. 7. Additional diaphragms act as additional sound sources in the wing surface.

A separate amplitude test maintained a constant speaker and diaphragm configuration and varied the amplitude directly from the sound amplifier. Five speakers centered about midspan at $c' = 0.1$ were forced at $f_e = 800$ Hz ($St^* = 0.029$). The speaker and diaphragm configuration is shown in Fig. 12. Figure 12 shows that $\Delta(L/D)$ is a simple function of forcing amplitude, with measured acoustic power at the shear layer $A_3 < A_2 < A_1$.

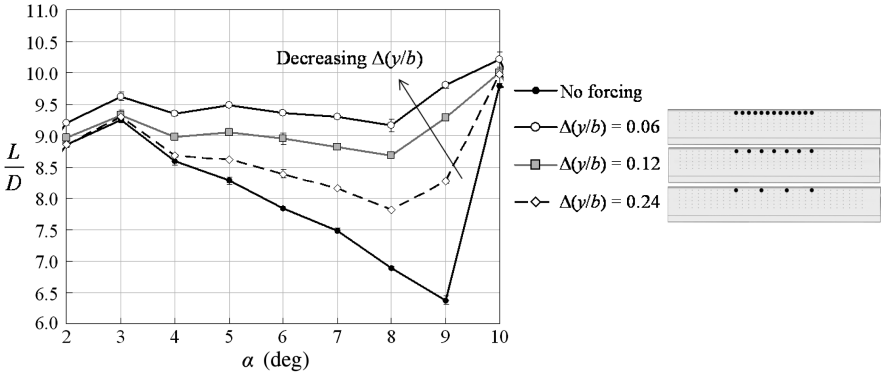

Fig. 9 L/D for the E387 wing at $Re = 60{,}000$ with activated speakers at $c' = 0.1$ between $-0.36 \le y/b \le 0.36$ with different spacings. $f_e = 850$ Hz ($St^* = 0.031$).

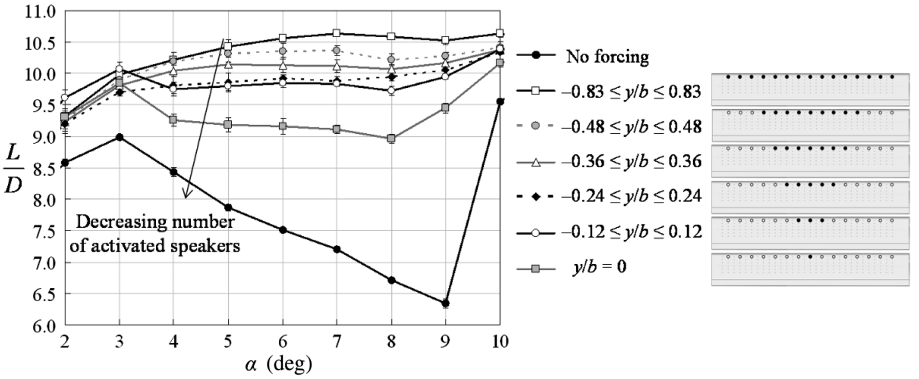

Fig. 11 L/D **at** $Re = 60{,}000$ **for various activated speakers and constant number of diaphragms.** $f_e = 800$ **Hz** ($St^* = 0.029$)**. Black circles are activated speakers, white circles inactivated speakers.**

E. Localized Excitation

While maintaining the same diaphragm configuration, activating nine speakers between $-0.48 \le y/b \le 0.48$ (curve b in Fig. 13) yields the same result within measurement uncertainty as activating five speakers within the same span, where the spacing between speakers is doubled (curve c in Fig. 13), and electrical power input is almost halved. This economy is not unexpected because extra diaphragms act as additional sound sources, albeit at reduced amplitude. However, when the holes over the inactivated speakers were blocked, resulting in only five total diaphragms (one for each speaker), the L/D improvements were significantly lower (curve d in Fig. 13). Curve d lies between the curve associated with the nominal, unexcited state (curve a) and the dome-shaped L/D curves associated with the high-lift state (curves b and c).

Raw particle images can be used to mark a dark separation line as particle-poor fluid from the boundary layer is released into the otherwise uniform exterior distribution. These images can be used to directly infer flow conditions on the wing. Figure 14 shows the raw PIV images for the four cases labeled a–d in Fig. 13 at $\alpha = 9$ deg. Activated speakers are indicated by solid black circles, inactivated speakers with diaphragms over them are indicated by white circles, and solid wing sections (i.e., where holes are filled in) have no special marker. Arrows show the streamwise position where the dark separation lines can no longer be readily distinguished from the background.

At a span station over an activated speaker (Figs. 14b–14d), the dark separation line ends at $x/c \approx 0.5$, followed by dark patches that mark distinct vortical structures, which undersampled time series show have a very regular passage frequency. Over a solid portion of the wing, the end of the separation line is farther downstream ($x/c \approx 0.6$) and is not followed by distinct vortical structures (Figs. 14a–14d).

When no speakers are activated, as in Fig. 14a, the visible separation line also ends at the farther-downstream location ($x/c \approx 0.6$) across both solid wing sections and diaphragms. The alternating pattern of separation line ending points is the same in Figs. 14b and 14c, further indicating that diaphragms over inactivated speakers still act as sound sources. It is plausible that acoustic excitation amplifies a naturally occurring instability in the originally separated shear layer (Fig. 15a), returning high-speed fluid close to the surface. The forced vortical structures then move down the airfoil chord and result in a flow that is reattached, in the time-averaged sense (Fig. 15b).

The small differences in separation line stability and persistence of Fig. 14 are not easily resolved in PIV measurement, where scales smaller than a correlation box size are not observable, but the overall spanwise vorticity distributions for forced and unexcited flows are similar to previous measurements in globally forced experiments [6]. Figure 16a shows that, at $\alpha = 9$ deg, the natural state is SI, where the flow separates close to the half-chord and does not reattach. The gradual forward movement of the separation line from close to the trailing edge at low α accounts for the increase in drag and rather small lift increments as α increases. In Fig. 16b, the flow is acoustically forced at $f_e = 800$ Hz and has switched to SII. A region of separated flow close to the leading edge is followed by reattachment, and so the global flow sees a wing with high effective camber. This is what leads to the higher lift and lower drag in SII.

F. Chordwise Location

The detailed instability mechanisms behind both forced and unforced flows described here are not necessarily simple to specify

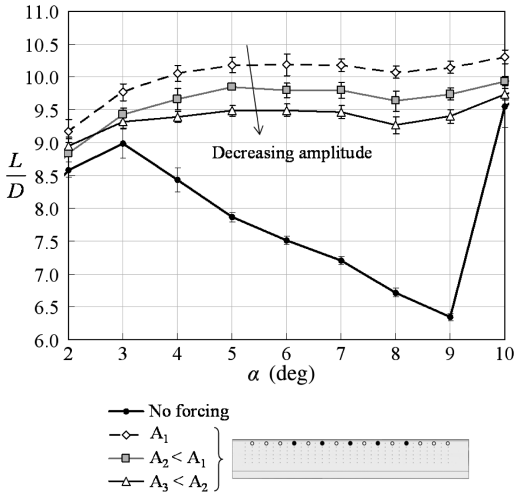

Fig. 12 Effect of varying amplitude for five activated speakers and 15 diaphragms covering $-0.83 \le y/b \le 0.83$ **at** $c' = 0.1$ **and forced at** $f_e =$ **800 Hz** ($St^* = 0.029$)**.**

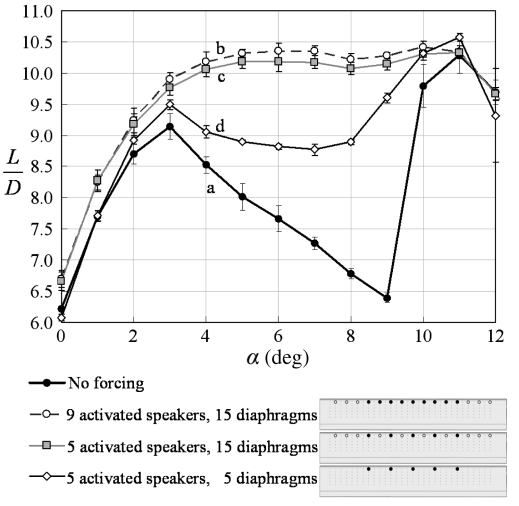

Fig. 13 L/D **at** $Re = 60{,}000$ **with activated speakers between** $-0.83 \le y/b \le 0.83$ **at** $c' = 0.1$**. Excitation with 15 diaphragms is at 800 Hz, 5 diaphragms is at 900 Hz.**

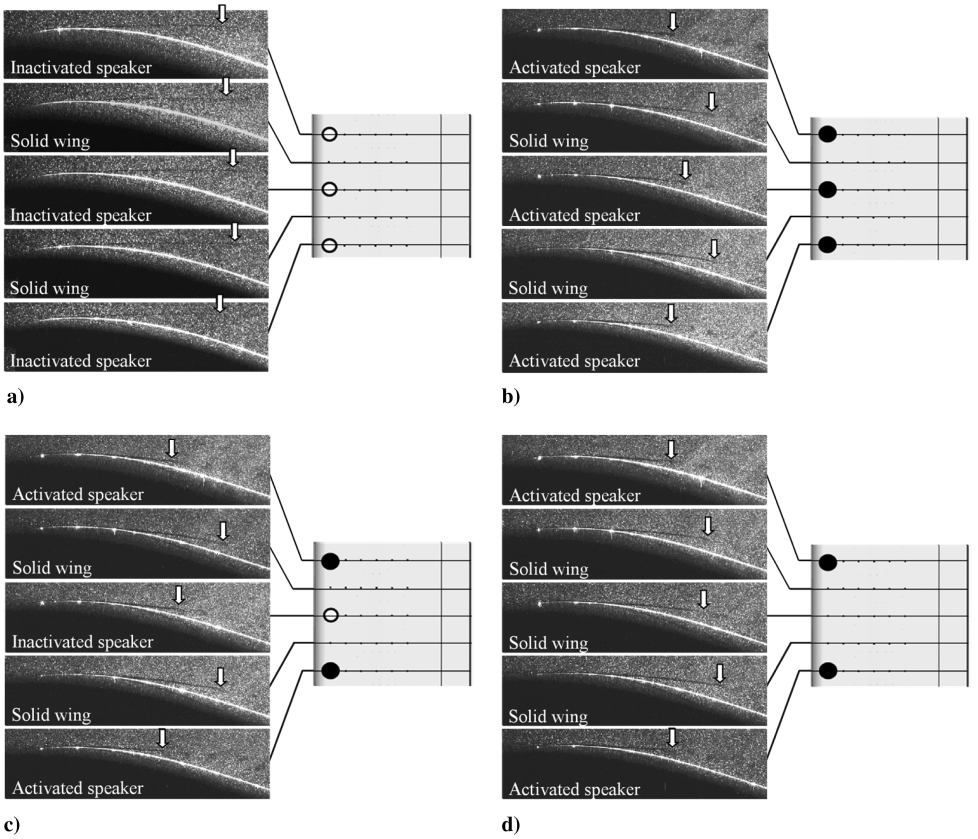

Fig. 14 PIV images for different span stations at $Re = 60{,}000$, $\alpha = 9$ deg with speakers at $c' = 0.1$, and $f_e = 900$ Hz with different activation conditions and spacing.

and not necessarily general to all cases. Possible receptive sites to finite amplitude disturbances include, from upstream to trailing edge, Tollmien–Schlichting waves in the attached laminar boundary layer, inflectional mean profiles in the bubble shear layer, Kelvin–Helmholtz-type instabilities in the separated shear layer, and wake profile instabilities aft of the trailing edge (TE). Moreover, there can be acoustically propagated feedback from the TE back to any one of the upstream modes, altering the incoming flow state [3,4,20,21]. More detailed investigation of the natural and forced mean flow profiles will follow later, but here we show initial evidence on the effect of chordwise-local acoustic forcing.

Six rows of five speakers over $-0.48 \le y/b \le 0.48$ spaced $\Delta(y/b) = 0.24$ apart were excited. The six rows of speakers were located at $c' = 0.1, 0.2, 0.3, 0.4, 0.5, 0.6$. An example of this speaker configuration (at $c' = 0.1$) is shown in the wing schematic associated with curve d in Fig. 13. The holes over inactivated speakers were blocked so that the diaphragms corresponded only to activated speakers. At $\alpha = 9$ deg, each row of speakers was individually forced over a sweep of frequencies, and the resulting $\Delta(L/D)$ is shown in Fig. 17.

The largest range of effective f_e occurs at $c' = 0.1$, where $\Delta(L/D) \approx 50\%$. For rows of speakers at $c' > 0.1$, the range of effective f_e is much narrower. The range of f_e where $L/D > 1/2L/D_{\max}$ can be denoted as R and is plotted for different c' in Fig. 18a. R decreases with increasing c' until $c' = 0.5$, where R is approximately the same between $0.4 \le c' \le 0.6$. In general, the magnitude of the maximum $\Delta(L/D)$ decreases with downstream row location, as shown in Fig. 18b. $\Delta(L/D)$ is constant for $c' = 0.4$ and 0.5 but then slightly increases at $c' = 0.6$.

Thus far, measurements show that acoustic sources located close together, across the entire span, and nearest to the leading edge of the wing cause the highest increase in $\Delta(L/D)$. A subsequent study was done to determine if the number of acoustic sources alone was a major

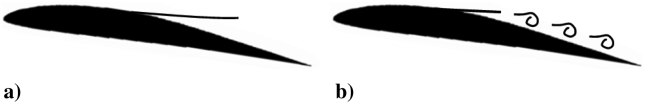

Fig. 15 Schematic of the separation line a) for unexcited flow (SI) and b) excited flow (SII), where separation occurs slightly earlier and the separation line vanishes earlier as vortical structures form.

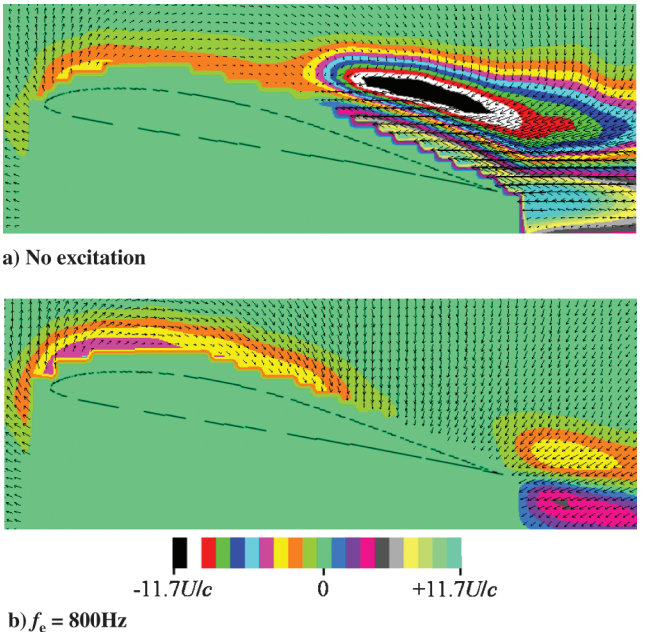

Fig. 16 $\omega_y(x,z)$ superimposed on fluctuating velocity vector fields at $y/b = 0$ a) without excitation and b) with excitation ($f_e = 800$ Hz), $Re = 60{,}000$, $\alpha = 9$ deg.

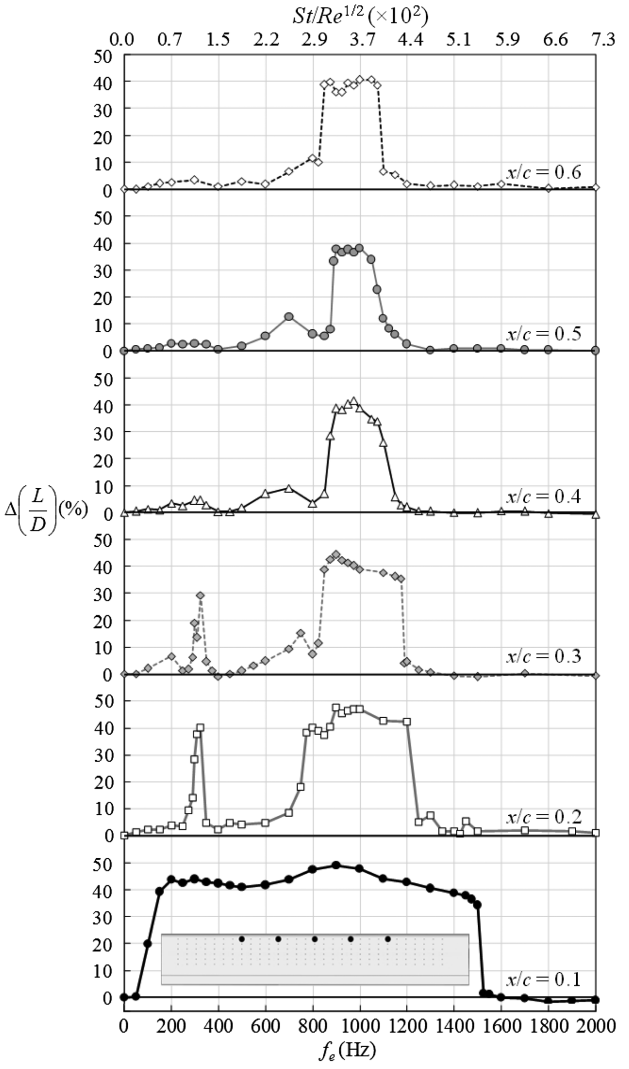

Fig. 17 $\Delta(L/D)$ for various f_e for five speakers spaced $\Delta(y/b) = 0.24$ apart between $-0.83 \le y/b \le 0.83$ at different c' locations. $Re = 60{,}000$, and $\alpha = 9$ deg.

factor in effective excitation. Measurements of $\Delta(L/D)$ were taken at $c' = 0.1$ for two other speaker configurations where a constant number of speakers was maintained, but the spacing between speakers was varied. Figure 19 shows the effect of varying the speaker spacing, $\Delta(y/b)$, on $\Delta(L/D)$ for the wing at $Re = 60,000$ and $\alpha = 9$ deg at select frequencies. For almost all f_e values, a simple correlation exists for $\Delta(L/D)$ versus $\Delta(y/b)$. For a given power input (a constant number of activated speakers), a larger spacing between acoustic sources yields a larger improvement in wing performance, implying that the number of acoustic sources alone does not influence the flow but rather the distribution of these acoustic sources.

G. Combined Effect of Holes and Internal Forcing

Open holes in the suction surface of the wing drive the flow to the high-lift state through passive resonance [15]. Covering the holes with thin diaphragms removes this effect, as shown in Fig. 20. Individually, the effect of open holes and the effect of internal acoustic forcing both improve wing performance. At $Re = 40,000$, neither of these methods by themselves produces dome-shaped L/D curves, such as those at $Re = 60,000$ (i.e., Fig. 6b).

In the α region of interest (5–12 deg), a local minimum in L/D occurs at $\alpha = 7$ deg, as seen in Fig. 20. At this α, a row of 15 speakers at $c' = 0.1$ was forced at varying f_e, and the corresponding $\Delta(L/D)$ are shown in Fig. 21. In the case of pure internal acoustic excitation at $Re = 40,000$ and $\alpha = 9$ deg (Fig. 5), a single peak in L/D occurs at $f_e \approx 500$ Hz ($St^* \approx 0.034$). However, in the case of both open holes and internal acoustic excitation, the range of effective f_e is much wider ($f_e = 100500$ Hz or $St^* = 0.0070.034$).

When the speakers were forced at $f_e = 200$ Hz without diaphragms in the lid of the wing, the combined effect of active acoustic forcing plus open holes gives the highest L/D increase, and the resulting dome-shaped L/D curve is shown in Fig. 22. In the same figure, L/D associated with diaphragms and no forcing, open holes and no forcing, and pure internal acoustic forcing at $c' = 0.1$ are also plotted. The performance of the wing with open holes only and with pure internal acoustic forcing are nearly the same, supporting the idea that forcing through a passive Helmholtz resonator mechanism and an equivalent active acoustic source are equivalent. The L/D curves for these two cases lie between the two extremes of closed holes without forcing and open holes with forcing. At $Re = 40,000$, pure internal acoustic excitation does not yield a completely high-lift state, but removing the diaphragms allows the high-lift state to be achieved.

IV. Discussion

A. Localized Separation Control

Besides separating the phenomena associated with pure internal acoustic forcing from those associated with acoustic resonance due to open holes, the results reported here provide a study of spatially localized acoustic forcing, which was not achievable with the wing-speaker arrangements used previously. Here, local spanwise flow separation evidently different in locations where there are speakers, diaphragms, or just a solid surface. The presence of a local acoustic source changes the flow separation quasi-locally, and the amplitude and symmetry of variations in L/D can be selected by appropriate selection of forcing pattern geometry.

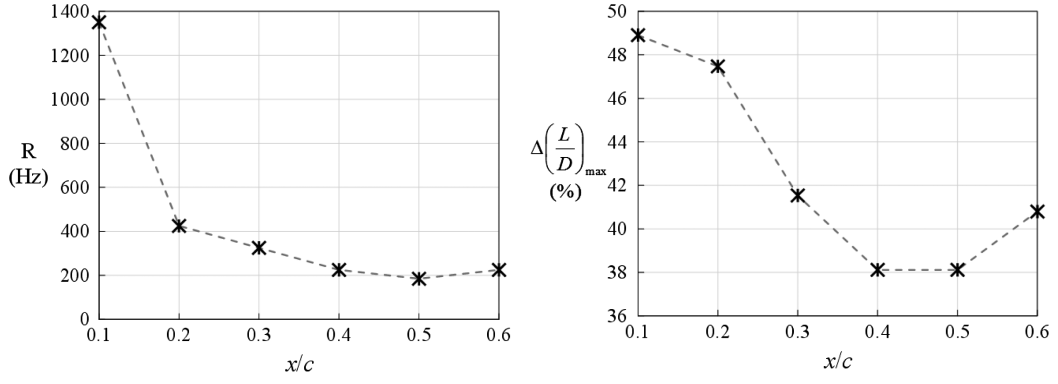

a) b)

Fig. 18 a) R, the range of f_e where $L/D > 1/2L/D_{max}$, and b) $\Delta(L/D)_{max}$ at different x/c for five speakers spaced $\Delta(y/b) = 0.24$ apart between $-0.83 \le y/b \le 0.83$ at $Re = 60,000$, and $\alpha = 9$ deg.

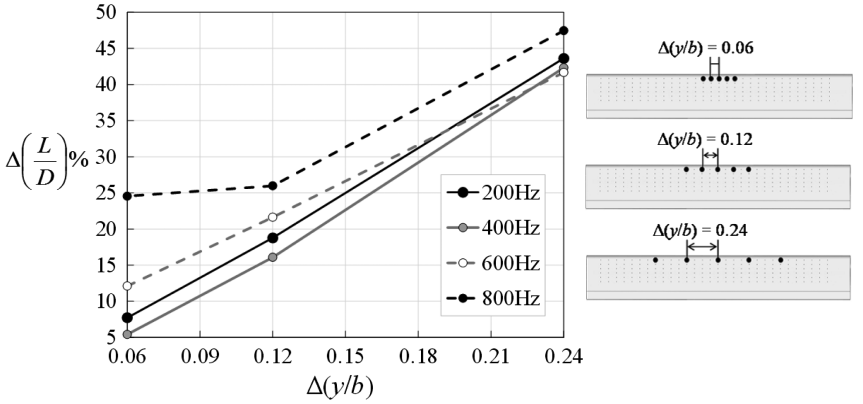

Fig. 19 $\Delta(L/D)$ at select frequencies for different speaker spacing $\Delta(y/b)$, at $Re = 60{,}000$ and $\alpha = 9$ deg. Five speakers are located at $c' = 0.1$.

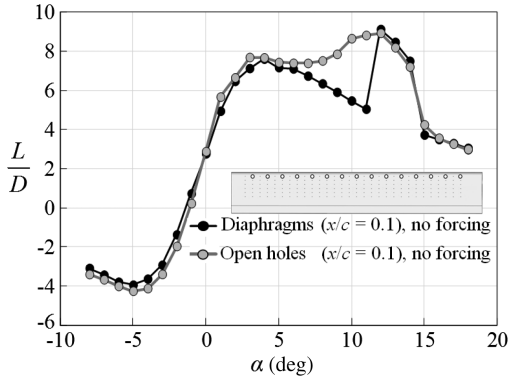

Fig. 20 L/D curves at $Re = 40{,}000$ for inactivated speakers with diaphragms and open holes at $c' = 0.1$.

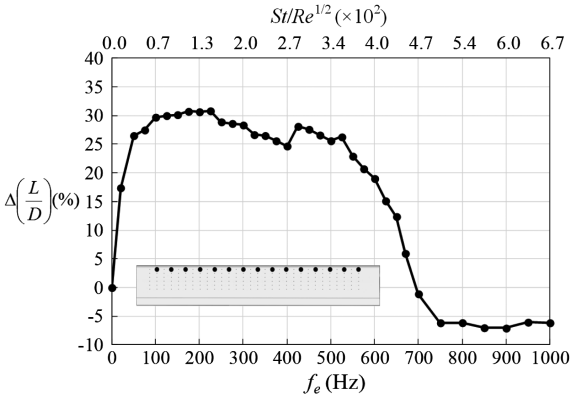

Fig. 21 $\Delta(L/D)$ at various f_e for the wing with open holes at $c' = 0.1$ at $Re = 40{,}000$ and $\alpha = 7$ deg.

Most previous internal acoustic forcing studies were for higher $Re(> 2 \times 10^5)$ [7–11], and none used wing profiles having bistable state behavior like the E387 airfoil. However, the bistable state is actually common for many smooth airfoils for $Re < 10^5$, and during cruise conditions (at low, prestall α), these airfoils could naturally experience abrupt changes in aerodynamic efficiency. This is why airfoil selection is so critical at moderate Re, and this paper shows how the potentially catastrophic, abrupt changes in both L and D can be controlled, locally on the wing.

Ultimately, the purpose of the local acoustic forcing is to selectively amplify intrinsic flow instabilities so as to efficiently exert a strong influence on the flow through a small control amplitude, measured in acoustic power, or electrical drain on a battery. We are also interested in using the local flow control to understand further which instability mechanisms are most receptive and under which conditions. This paper presents the acoustic forcing results only, and further work needs to be done to link this more closely with the various possible instability modes and amplification mechanisms.

B. Facility Independence

The internal acoustic excitation results reported here differ from earlier reported external acoustic excitation results on the same wing [6]. The most prominent differences in wing performance can be seen in the L/D versus f_e graphs (Fig. 23). At $Re = 60{,}000$, the $\Delta(L/D)(f_e)$ curve from external forcing is discontinuous, showing particular preferential f_e values that increase L/D, whereas the equivalent curve from internal forcing is continuous, showing that all values of f_e within a given range will increase L/D. Results from the external forcing study determined a dependence of optimum f_e on wind-tunnel resonances, which explains why only a selection of f_e values improve wing L/D. There is no such dependence for internal acoustic forcing, and so this efficiency enhancement and separation control technique can, in principle, be applied to standard flying devices in open flight.

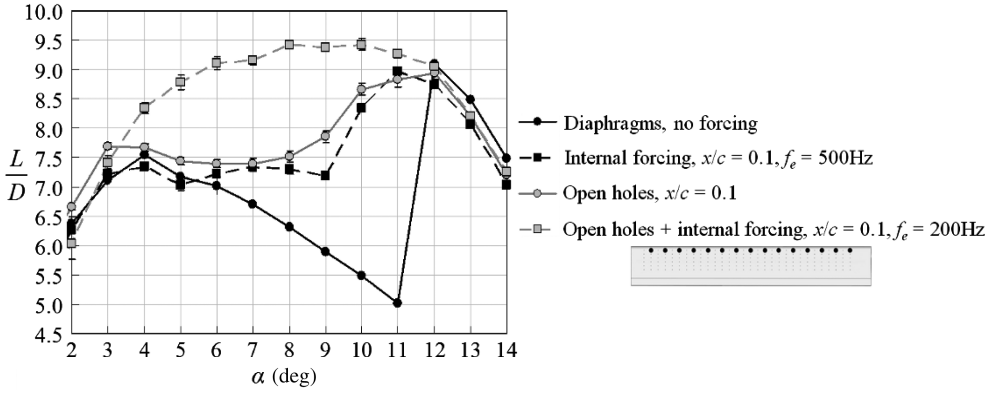

Fig. 22 Combined effect of open holes and acoustic forcing at $Re = 40{,}000$.

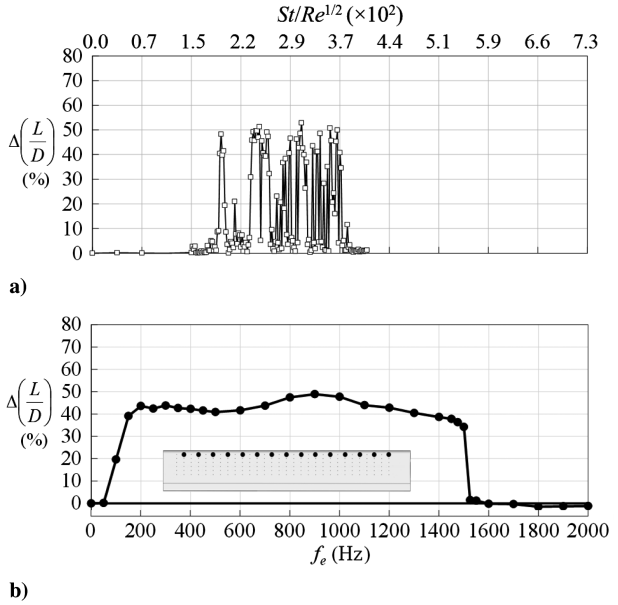

Fig. 23 $\Delta(L/D)$ of the E387 wing a) with external acoustic forcing at $\alpha = 8$ deg (replotted from Yang et al. [6]) and b) with internal acoustic forcing from 15 speakers at $c' = 0.1$ at $\alpha = 9$ deg.

C. Spanwise Slots

All previous studies of internal acoustic excitation have used a single speaker lying beneath an uncovered spanwise channel or slit in the wing [7–11]. Some of the wing models [7] contained not only uncovered spanwise slits but also additional pressure taps along the suction surface. In light of the study by Yang and Spedding on Helmholtz resonance from open holes [6], there is reason to question the validity of the true nominal performance of any wing with open cavities regardless of Re because the resonance mechanism is independent of flow speed.

The modifications in wing performance previously observed in the literature may have originated, not from pure internal acoustic excitation, but from a combination of acoustic resonance and internal forcing effects, as observed here (e.g., Fig. 22). Although most previous studies were for airfoils and wings at large, poststall α, when Helmholtz resonance would be unimportant, at lower α, it is quite likely that a combined resonance and internal forcing phenomenon would cause the observed changes in wing performance.

V. Conclusions

There is a particular practical range of flight Reynolds number, $10^4 \leq Re \leq 10^5$, where, at prestall α, the flow over the suction surface of an airfoil or finite wing can suddenly switch states, which are called SI and SII. In SI, the laminar boundary layer simply separates at some point before the trailing edge. In SII, separation is closer to the leading edge, and reattachment occurs following a laminar separation bubble. SII is associated with much higher L/D than SI. Here, it is shown that local acoustic forcing can be used to selectively control local flow separation, and combinations of active and passive acoustic forcing allow access to an envelope of $L/D(\alpha)$ curves. Special care must be taken to separate out these two contributors, which have often been combined in the literature. Local acoustic forcing appears to be effective in modifying the flow, but the mechanism is not yet clear. Future work on calculating unstable modes of both attached and separated flow profiles will help, and further practical steps include measuring the roll moments on a wing under asymmetric internal acoustic forcing. With proper spacing, frequency, and amplitude selection, small embedded speakers could replace movable control surfaces for small-scale flying devices.

Acknowledgments

This research was supported through a National Science Foundation fellowship and U.S. Air Force Office of Scientific Research grant FA 9550-11-1-0106, together with internal University of Southern California grants for undergraduate research and the Rose Hills Foundation.

References

[1] Alam, M., and Sandham, N. D., "Direct Numerical Simulation of 'Short' Laminar Separation Bubbles with Turbulent Reattachment," *Journal of Fluid Mechanics*, Vol. 410, 2000, pp. 1–28. doi:10.1017/S0022112099008976

[2] Alam, M., and Sandham, N. D., "Mechanisms of Transition and Heat Transfer in a Separation Bubble," *Journal of Fluid Mechanics*, Vol. 403, 2000, pp. 223–250. doi:10.1017/S0022112099007119

[3] Marxen, O., and Rist, U., "Mean Flow Deformation in a Laminar Separation Bubble: Separation and Stability Characteristics," *Journal of Fluid Mechanics*, Vol. 660, 2010, pp. 37–54. doi:10.1017/S0022112010001047

[4] Marxen, O., and Henningson, D. S., "The Effect of Small Amplitude Convective Disturbances on the Size and Bursting of a Laminar Separation Bubble," *Journal of Fluid Mechanics*, Vol. 671, 2011, pp. 1–33. doi:10.1017/S0022112010004957

[5] Marxen, O., Lang, M., and Rist, U., "Discrete Linear Local Eigenmodes in a Separating Laminar Boundary Layer," *Journal of Fluid Mechanics*, Vol. 711, 2012, pp. 1–26. doi:10.1017/jfm.2012.263

[6] Yang, S. L., and Spedding, G. R., "Separation Control by External Acoustic Excitation on a Finite Wing at Low Reynolds Numbers," *AIAA Journal*, Vol. 51, No. 6, 2013, pp. 1506–1515.

[7] Hsiao, F. B., Jih, J. J., and Shyu, R. N., "The Effect of Acoustics on Flow Passing a High-AOA Airfoil," *Journal of Sound and Vibration*, Vol. 199, No. 2, 1997, pp. 177–188. doi:10.1006/jsvi.1996.0618

[8] Hsiao, F. B., Jih, J. J., and Shyu, R. N., "Control of Wall-Separated Flow by Internal Acoustic Excitation," *AIAA Journal*, Vol. 28, No. 8, 1989, pp. 1440–1486.

[9] Chang, R. C., Hsiao, F. B., and Shyu, R. N., "Forcing Level Effects of Internal Acoustic Excitation on the Improvement of Airfoil Performance," *Journal of Aircraft*, Vol. 29, No. 5, 1992, pp. 823–829.

[10] Huang, L. S., Maestrello, L., and Bryant, T. D., "Separation Control Over an Airfoil at High Angles of Attack by Sound Emanating From the Surface," *19th AIAA, Fluid Dynamics, Plasma Dynamics, and Lasers Conference*, AIAA Paper 1987-1261, June 1987.

[11] Huang, L. S., Bryant, T. D., and Maestrello, L., "The Effect of Acoustic Forcing on Trailing Edge Separation and Near Wake Development of an Airfoil," *1st National Fluid Dynamics Congress*, AIAA Paper 1988-3531, July 1988.

[12] Zabat, M., Farascaroli, S., Browand, F., Nestlerode, M., and Baez, J., "Drag Measurements on a Platoon of Vehicles," *Research Reports, California Partners for Advanced Transit and Highways (PATH)*, Inst. of Transportation Studies, Univ. of California, Rept. UCB-ITS-PRR-93-27, Berkeley, Berkeley, CA, 1994.

[13] McArthur, J., "Aerodynamics of Wings at Low Reynolds Numbers," Ph.D. Dissertation, Dept. of Aerospace and Mechanical Engineering, Univ. of Southern California, Los Angeles, CA, 2007.

[14] Spedding, G. R., and McArthur, J., "Span Efficiencies of Wings at Low Reynolds Number," *Journal of Aircraft*, Vol. 47, No. 1, pp. 120–128, 2011. doi:10.2514/1.44247

[15] Yang, S. L., and Spedding, G. R., "Passive Separation Control by Acoustic Resonance," *Experiments in Fluids*, Vol. 54, No. 10, 2013, pp. 1–16. doi:10.1007/s00348-013-1603-6

[16] Gaster, M., and Grant, T., "An Experimental Investigation of the Formation and Development of a Wave Packet in a Laminar Boundary Layer," *Proceedings of the Royal Society A: Mathematical, Physical and Engineering Sciences*, Vol. 347, No. 1649, 1975, pp. 253–269. doi:10.1098/rspa.1975.0208

[17] Schlichting, H., *Boundary Layer Theory*, Springer, New York, 1968, pp. 38–48.

[18] Lin, J. C. M., and Pauley, L. L., "Low-Reynolds Number Separation on an Airfoil," *AIAA Journal*, Vol. 34, No. 8, 1996, pp. 1570–1577. doi:10.2514/3.13273

[19] McAuliffe, B. R., and Yaras, M. I., "Transition Mechanisms in Separation Bubbles Under Low and Elevated Free Stream Turbulence," *Proceedings of the ASME Turbo Expo 2007*, American Society of Mechanical Engineering, New York, 2007, pp. 1–10.

[20] Diwan, S. S., and Ramesh, O. N., "On the Origin of the Inflectional Instability of a Laminar Separation Bubble," *Journal of Fluid Mechanics*, Vol. 629, 2009, pp. 263–298. doi:10.1017/S002211200900634X

[21] Jones, L. E., Sandberg, R. D., and Sandham, N. D., "Stability and Receptivity Characteristics of a Laminar Separation Bubble on an Aerofoil," *Journal of Fluid Mechanics*, Vol. 648, 2010, pp. 257–296. doi:10.1017/S0022112009993089

A. Naguib
Associate Editor